

Masked Generative Extractor for Synergistic Representation and 3D Generation of Point Clouds

Hongliang Zeng, Ping Zhang*, Fang Li, Jiahua Wang, Tingyu Ye and Pengteng Guo
South China University of Technology, Guangzhou, China
pzhang@scut.edu.cn

Abstract

Representation and generative learning, as reconstruction-based methods, have demonstrated their potential for mutual reinforcement across various domains. In the field of point cloud processing, although existing studies have adopted training strategies from generative models to enhance representational capabilities, these methods are limited by their inability to genuinely generate 3D shapes. To explore the benefits of deeply integrating 3D representation learning and generative learning, we propose an innovative framework called *Point-MGE*. Specifically, this framework first utilizes a vector quantized variational autoencoder to reconstruct a neural field representation of 3D shapes, thereby learning discrete semantic features of point patches. Subsequently, we design a sliding masking ratios to smooth the transition from representation learning to generative learning. Moreover, our method demonstrates strong generalization capability in learning high-capacity models, achieving new state-of-the-art performance across multiple downstream tasks. In shape classification, Point-MGE achieved an accuracy of 94.2% (+1.0%) on the ModelNet40 dataset and 92.9% (+5.5%) on the ScanObjectNN dataset. Experimental results also confirmed that Point-MGE can generate high-quality 3D shapes in both unconditional and conditional settings.

1 Introduction

Recent studies have confirmed that masked modeling-based representation learning frameworks [Yu *et al.*, 2022; Pang *et al.*, 2022; Zhang *et al.*, 2022b] can extract high-quality 3D representations. At the same time, generative models [Zhang *et al.*, 2022a; Mittal *et al.*, 2022; Zhang *et al.*, 2023a] have achieved remarkable success in generating realistic 3D shapes. Nevertheless, few studies have explored the deep integration of these two models to unlock their combined potential in 3D shape processing. In natural language

processing (NLP) [Touvron *et al.*, 2023] and 2D image domains [Li *et al.*, 2023], we have witnessed the versatility of pre-trained models: not only can they be used for diverse generative tasks such as question answering (QA), code generation, and image generation, but they can also serve as feature extractors for various downstream tasks through fine-tuning. These achievements prompt us to consider: can the benefits of this model integration be similarly applied to the representation of point cloud data and 3D shape generation? To this end, we conducted an in-depth analysis of the characteristics of both models and found that masked reconstruction methods offer a potential pathway to achieve this integration, though several challenges remain.

Firstly, generative learning is easily trained on discrete distributions, whereas existing point cloud representation learning [Pang *et al.*, 2022; Zhang *et al.*, 2022b] tends to operate within continuous feature spaces. In prior work, PointBert [Yu *et al.*, 2022] learns a tokenizer by reconstructing the input point cloud and optimizing the chamfer distance (CD) loss. However, using point clouds directly as the reconstruction target introduces a sampling bias. This is because 3D shapes are inherently continuous, but point clouds sampled from these shapes can only approximate them in a discrete form. This sampling bias can lead to non-zero loss differences between different point cloud samples of the same object, thereby affecting the precise understanding of shape features. Moreover, methods that rely solely on point cloud reconstruction are limited in capturing high-level representations of 3D shapes. For instance, they cannot generate richer shape descriptions such as neural radiance fields (NeRFs) or triangular meshes, which restricts the model’s potential in generative tasks. To address this, we shift the reconstruction target to 3D shapes represented by NeRFs and utilize a vector quantized variational autoencoder (VQVAE) [Van Den Oord *et al.*, 2017] to extract discrete semantic features from point clouds. The Point-MGE framework leverages these high-level semantic discrete features not only as input but also as reconstruction targets, thereby learning the probability distribution of masked tokens. During the vector quantization process, different point cloud samples from the same local region are consistently mapped to the same discrete tokens, ensuring consistency and robustness in the representations.

Secondly, the inherent unordered nature of point cloud poses a challenge for Transformer-based generative models,

*Corresponding author

as these models require serialized inputs. To address this issue, we partition the complete point cloud into multiple patches, each defined by a fixed number of points and a central point. To serialize these patches, we adopt the Morton sorting algorithm used in PointGPT [Chen *et al.*, 2023], which can sort point cloud patches while preserving geometric relationships. In generation task, since the central point of point cloud patch is unknown, we introduce relative position encoding in the generator of Point-MGE as a replacement for traditional absolute position encoding, and use the central points as the reconstruction target.

Finally, generative training tends to adopt higher masking ratios, or even full masking, whereas representation learning typically uses relatively low masking ratios. In 2D image processing, MAGE [Li *et al.*, 2023] achieves variable masking ratios by randomly sampling them from a Gaussian distribution, utilizing these variable ratios to perform the task. However, due to the irregularity of point cloud data and the lack of support from large-scale datasets, such drastic fluctuations in masking ratios may adversely affect model convergence. To address this issue, we have carefully designed a sliding masking ratio mechanism to smoothly adjust the masking ratio during training. Specifically, the masking ratio gradually increases as training iterations progress, facilitating a smooth transition from representation learning to generative training. We also conducted a comparative analysis of the effects of different sliding curves. Point-MGE can scale to high-capacity model training and has demonstrated outstanding performance across multiple benchmark datasets. It achieved an accuracy of 94.2% on the ModelNet40 dataset [Wu *et al.*, 2015] for shape classification and 92.9% on the ScanObjectNN dataset [Uy *et al.*, 2019]. Additionally, in the part segmentation task on the ShapeNet-Part dataset [Yi *et al.*, 2016], our method attained an average class Intersection over Union (IoU) of 85.0%. Furthermore, we also showcased the capability of the pre-trained model to generate realistic 3D shapes in both unconditional and conditional settings.

Our main contributions can be summarized as follows: (I) We propose Point-MGE, a unified framework for point cloud data representation learning and generative training that combines a two-stage training method with a sliding masking ratio design. (II) Point-MGE overcomes the variance issue in point cloud sampling and scales to high-capacity model training, setting a new SOTA benchmark for downstream tasks. (III) Point-MGE is capable of generating high-quality 3D shapes in both unconditional and conditional settings.

2 Related Works

Representation Learning for Point Clouds. In recent years, self-supervised frameworks for point cloud representation learning have made significant progress, forming two main model paradigms. Firstly, methods based on contrastive learning [Xie *et al.*, 2020b; Zhang *et al.*, 2021; Afham *et al.*, 2022] have played an important role in point cloud self-supervised learning. These methods can explore the intrinsic properties of point clouds, but they often rely on cross-modal information or teacher models, which undoubtedly

add extra burden to the training process. Secondly, inspired by natural language processing [Devlin *et al.*, 2018; Brown *et al.*, 2020] and 2D computer vision [He *et al.*, 2022; Wei *et al.*, 2022], a more closely related area to our work is another category of methods based on masked point cloud modeling [Yu *et al.*, 2022; Pang *et al.*, 2022; Zhang *et al.*, 2022b; Chen *et al.*, 2023]. Point-M2AE [Zhang *et al.*, 2022b] proposed an innovative hierarchical transformer structure, extending Point-MAE [Pang *et al.*, 2022] to capture multi-scale features of point clouds. On the other hand, PointGPT [Chen *et al.*, 2023] attempts to solve the problem of global shape leakage through autoregressive generation, but it does not have the ability to generate high-quality 3D models from scratch. Additionally, methods based on masked region reconstruction are susceptible to point cloud sampling variance, which may introduce additional understanding and bias issues. To overcome these challenges, our method adopts a strategy of masked modeling in the high-level semantic space, effectively addressing the aforementioned issues.

Generative Models for 3D Shapes. In the field of 3D generation, generative adversarial networks (GANs) [Achlioptas *et al.*, 2018; Chen and Zhang, 2019; Ibing *et al.*, 2021; Zheng *et al.*, 2022] constitute a major generative paradigm, despite their limitations in training stability and mode collapse issues. Meanwhile, some research has turned to alternative approaches such as normalizing flows (NFs) [Dinh *et al.*, 2014; Rezende and Mohamed, 2015; Yang *et al.*, 2019], energy-based models (EBMs) [Xie *et al.*, 2016; Xie *et al.*, 2020a; Xie *et al.*, 2021], and autoregressive models (ARs) [Mittal *et al.*, 2022; Cheng *et al.*, 2022; Yan *et al.*, 2022; Zhang *et al.*, 2022a]. Recently, inspired by the significant progress of diffusion models (DMs) [Dhariwal and Nichol, 2021] in image synthesis, some studies have begun to explore the application of diffusion models to 3D shape generation [Zhou *et al.*, 2021; Vahdat *et al.*, 2022; Hui *et al.*, 2022; Shue *et al.*, 2023; Chou *et al.*, 2023; Zhang *et al.*, 2023a]. Although these models can generate realistic 3D models, they often lack the ability to extract high-quality semantic representations from 3D shapes, limiting their direct application in point cloud representation learning tasks. To address this challenge, we propose an innovative approach aimed at generating diverse samples while extracting high-quality semantic embeddings from 3D shapes to promote data generalization and enhance the performance of downstream tasks.

3 Method

Point-MGE is designed as a unified framework for both 3D generation tasks and representation learning. As shown in Figure 1, the framework first divides the input point cloud into multiple local point patches and serializes them based on their geometric positional relationships. Then, it uses a mini-PointNet [Qi *et al.*, 2017a] model for initial feature extraction of each point patch. Subsequently, by training a VQVAE model, these features are quantized into discrete tokens. Finally, the framework combines a variable masking ratio with a vision transformer (ViT)-based extractor-generator architecture to predict masked tokens.

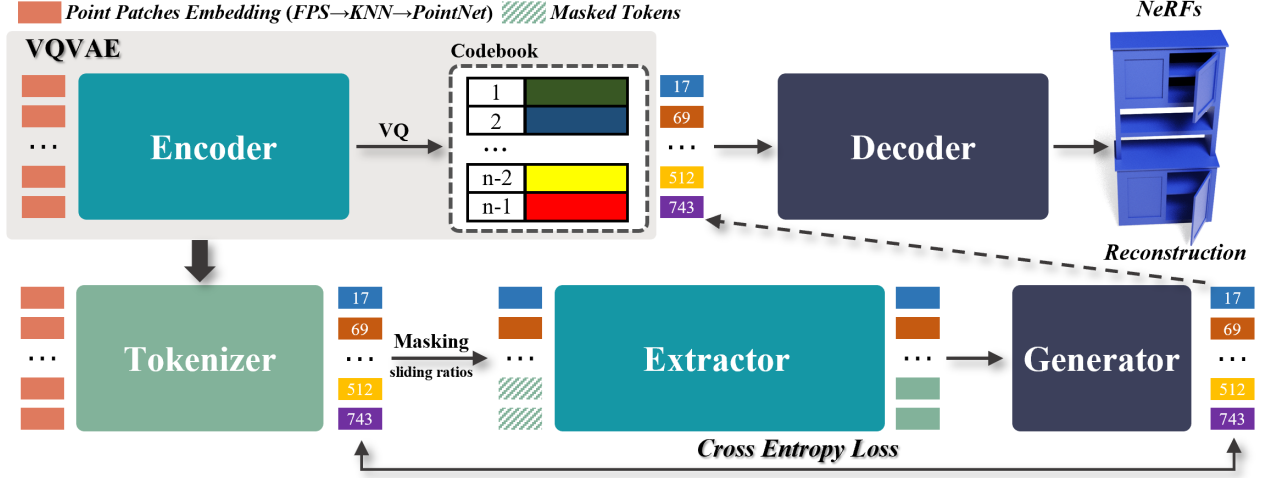


Figure 1: **Overall pipeline of Point-MGE.** First, a VQVAE is used to reconstruct 3D shapes represented by NeRFs, converting the input point cloud into a series of discrete semantic tokens. Then, where a ViT-based extractor-generator architecture is employed to extract high-quality feature representations from the unmasked tokens and to reconstruct the masked tokens.

3.1 Point Patch Embedding

Point Cloud Patching. We determine the number of patches and the number of points per patch in the point cloud sampling process through two key hyperparameters G and K . Specifically, given the input point cloud $X \in \mathbb{R}^{n \times 3}$, we use the farthest point sampling (FPS) strategy to select G central points,

$$C = \{x_i\}_{i \in \mathcal{N}} = \text{FPS}(X), C \in \mathbb{R}^{G \times 3}, \quad (1)$$

where $|\mathcal{N}| = n$. Then, using the K-nearest neighbors (KNN) algorithm, we identify $|\mathcal{N}_i| = K$ neighbors of the central point $\{x_i\}_{i \in \mathcal{N}}$, resulting in G point cloud patches,

$$P = \{x_j\}_{j \in \mathcal{N}_i} = \text{KNN}(C, X), P \in \mathbb{R}^{G \times K \times 3}. \quad (2)$$

Embedding. To provide serialized input, we follow [Chen *et al.*, 2023] and encode the coordinates of the central points x_i into one-dimensional space using morton ordering [Morton, 1966], and then sort them to obtain serialized central points $C^s \in \mathbb{R}^{G \times 3}$ and point cloud patches $P^s \in \mathbb{R}^{G \times 3}$. We project each patch into an embedding vector using the mini-PointNet[Qi *et al.*, 2017a] module,

$$P_E^s = \{e_i\}_{i \in \mathcal{G}} = \text{PointNet}(P^s), P_E^s \in \mathbb{R}^{G \times D}, \quad (3)$$

where $|\mathcal{G}| = G$, D is the embedding dimension of the point patch.

3.2 Tokenization

We train a VQVAE [Van Den Oord *et al.*, 2017] to obtain a quantizer that embeds input point patches into a series of semantic tokens. This tokenization step enables our model to focus on high-level semantics, which helps to overcome the variance issue in point cloud sampling and allows for a more comprehensive understanding of 3D shapes.

Vector Quantization. We use a ViT-based encoder to learn the local latents T . The input to the transformer includes the sorted point block embeddings P_E^s and the sinusoidal positional encodings [Vaswani *et al.*, 2017] C_E^s of the center point,

$$T = \{t_i\}_{i \in \mathcal{G}} = \text{Enc}(P_E^s, C_E^s), T \in \mathbb{R}^{G \times D}. \quad (4)$$

The output of the encoder is then replaced with the closest vector in the codebook \mathcal{Q} through vector quantization,

$$T^Q = \{t_i^q\}_{i \in \mathcal{G}} = \arg \min_{t_j^q \in \mathcal{Q}} \|t_j^q, t_i\|, T^Q \in \mathbb{R}^{G \times D}. \quad (5)$$

Reconstruction. We utilize a ViT-based decoder to reconstruct the 3D shape's NeRFs $\hat{\mathcal{O}}(x) \in \{0, 1\}$, where $\hat{\mathcal{O}}(x) = 1$ indicates that the point x in space belongs to the object. The decoder takes as input the quantized tokens and the position encoding of the center points,

$$T^D = \{t_i^d\}_{i \in \mathcal{G}} = \text{Dec}(T^Q, C_E^s), T^D \in \mathbb{R}^{G \times D}. \quad (6)$$

For any $x \in \mathbb{R}^3$, we use the nadaraya-watson estimator for interpolation to obtain its latent t_x^d . Then, we estimate $\mathcal{O}(x)$ through a multi-layer perceptron and a sigmoid activation function,

$$\mathcal{O}(x) = \text{Sigmoid}(\text{MLP}(x, t_x^d)). \quad (7)$$

The optimization objective consists of binary cross-entropy (BCE) loss and an additional commitment loss,

$$\mathcal{L}_n = \mathbb{E}_{x \in \mathbb{R}^3} [\text{BCE}(\mathcal{O}(x), \hat{\mathcal{O}}(x))] + \lambda \mathbb{E}_{x \in \mathbb{R}^3} [\mathbb{E}_{i \in \mathcal{M}} \|\epsilon(t_i^q) - t_i\|^2], \quad (8)$$

where $\epsilon(\cdot)$ represents the stop-gradient operation. In this paper, $\lambda = 0.25$ is a weighting coefficient.

3.3 Pre-training

After obtaining the tokenizer, we simultaneously train an extractor and a generator model through masking modeling. Below, we introduce the masking strategy, model design, and optimization objectives of Point-MGE.

Methods	Reference	Params(M)	ModelNet40		ScanObjectNN		
			w/o Vote	w/ Vote	OBJ_BG	OBJ_ONLY	PB_T50_RS
<i>Supervised Learning Only</i>							
PointNet [Qi <i>et al.</i> , 2017a]	CVPR 2017	3.5	-	89.2	73.3	79.2	68.0
PointNet++ [Qi <i>et al.</i> , 2017b]	Neurips 2017	1.5	-	90.7	82.3	84.3	77.9
DGCNN [Wang <i>et al.</i> , 2019]	TOG 2019	1.8	-	92.9	82.8	86.2	78.1
PointMLP [Ma <i>et al.</i> , 2022]	ICLR2022	12.6	94.1	94.5	-	-	85.2
P2P-HorNet [Wang <i>et al.</i> , 2022]	NeurIPS 2022	195.8	94.0	-	-	-	89.3
<i>with Single-Modal Pre-Training</i>							
Point-BERT [Yu <i>et al.</i> , 2022]	CVPR 2022	22.1	92.7	93.2	87.4	88.1	83.1
Mask-Point [Liu <i>et al.</i> , 2022]	ECCV 2022	22.1	-	93.8	89.3	88.1	84.3
Point-MAE [Pang <i>et al.</i> , 2022]	ECCV 2022	22.1	93.2	93.8	90.0	88.2	85.2
Point-M2AE [Zhang <i>et al.</i> , 2022b]	Neurips 2022	15.3	93.4	94.0	91.2	88.8	86.4
PointGPT [Chen <i>et al.</i> , 2023]	Neurips 2023	19.5	-	94.0	91.6	90.0	86.9
GPM [Li <i>et al.</i> , 2024]	CVPR2024	41.5	94.0	94.3	90.2	90.0	84.8
Point-MGE	-	15.3	93.8	94.2	92.9	91.0	87.1
<i>Improvement (baseline: Point-BERT)</i>	-	-	<i>+1.1</i>	<i>+1.0</i>	<i>+5.5</i>	<i>+2.9</i>	<i>+4.0</i>
Point-MAE-B [Pang <i>et al.</i> , 2022]	ECCV 2022	120.1	-	94.2	94.2	93.9	90.2
Point-M2AE-B [Zhang <i>et al.</i> , 2022b]	Neurips 2022	77.5	-	94.3	95.2	94.3	91.2
PointGPT-B [Chen <i>et al.</i> , 2023]	Neurips 2023	82.1	-	94.4	95.8	95.2	91.9
Point-MGE-B	-	77.5	-	94.5	96.1	95.7	92.3
<i>with Cross-Modal Pre-Training</i>							
ACT [Dong <i>et al.</i> , 2023]	ICLR 2023	22.1	93.2	93.7	93.3	91.9	88.2
Joint-MAE [Guo <i>et al.</i> , 2023]	IJCAI 2023	-	-	94.0	90.9	88.9	86.1
I2P-MAE [Zhang <i>et al.</i> , 2023b]	CVPR 2023	15.3	93.7	94.1	94.2	91.6	90.1
Recon [Qi <i>et al.</i> , 2023]	ICML 2023	44.3	94.1	94.5	95.2	93.3	90.6

Table 1: **Shape classification results on ModelNet40 [Wu *et al.*, 2015] and ScanObjectNN [Uy *et al.*, 2019].** We report the accuracy (%) of both training from scratch and fine-tuning models on ModelNet40 and ScanObjectNN datasets.

Masking Strategy. For a given point cloud $X \in \mathbb{R}^{n \times 3}$, we first use the trained tokenizer to obtain the corresponding discrete tokens T^Q . Subsequently, we introduce a sliding masking ratio to apply masking, which can be calculated as:

$$m_r = \beta + (1 - \beta) \left(\frac{\gamma}{\Gamma}\right)^u, \quad m_r \in [\beta, 1], \quad (9)$$

where, γ and Γ denote the current training iteration and the total number, respectively. The parameter $u > 0$ is a hyperparameter used to control the trend of the sliding function. After masking, to reduce training time and memory consumption, we randomly drop a portion of masked tokens, ensuring that only $V = (1 - \beta) \times G$ tokens are input to the extractor.

Extractor and Generator. We feed the remaining tokens into the ViT-based extractor-generator structure. Then, we concatenate a learnable mask token to the input sequence. The extractor processes the input tokens T_m^Q and encodes them into the latent feature space,

$$T^E = \{t_i^e\}_{i \in \mathcal{G}, m_i=0} = \text{Ext}(T_m^Q, C_E^s), \quad T^E \in \mathbb{R}^{V \times D}, \quad (10)$$

where $M = [m_i]_{i=1}^G$ represents a binary mask indicating whether a token is masked or not. Then, the output of the extractor is padded to the complete length G as the input T_p^E of the generator using the learnable mask token,

$$T^G = \{t_i^g\}_{i \in \mathcal{G}} = \text{Gen}(T_p^E, C_{RE}^s, \mathcal{C}), \quad T^G \in \mathbb{R}^{G \times D}, \quad (11)$$

where C_{RE}^s is the relative position encoding of the sorted center points C^s to adapt to the needs of the generation task, and \mathcal{C} is optional conditional information (e.g., category, image, and text).

Reconstructive Training. Our training target is to reconstruct the masked tokens along with the center point coordinates \hat{c}_i . The reconstruction of center points serves the generation task because our VQVAE decoder requires absolute position encoding as input to reconstruct 3D shapes. Our loss function consists of two parts: the cross-entropy loss for token reconstruction and the mean square error loss for center point reconstruction, which can be expressed as:

$$\mathcal{L}_{rt} = -\mathbb{E}_{t_i^q \in \mathcal{Q}} \left[\sum_{\forall i, m_i=1} \log p(t_i^q | T_m^G) \right] + \frac{1}{|M|} \sum_{\forall i, m_i=1} \|c_i, \hat{c}_i\|^2, \quad (12)$$

where T_m^G represents the masked portion of the tokens outputted by the generator.

3.4 Iterative Generation

After pretraining, following [Li *et al.*, 2023], we employ an iterative generation strategy to generate diverse 3D shapes. The generation process starts with all tokens being considered as masked tokens. Using a cosine function, we determine the number of masked tokens to be replaced in each iteration. Specifically, in each iteration, based on the predicted

Methods	5-way		10-way	
	10-shot	20-shot	10-shot	20-shot
<i>Supervised Learning Only</i>				
PointNet	52.0±3.8	57.8±4.9	46.6±4.3	35.2±4.8
PointNet-OcCo	89.7±1.9	92.4±1.6	83.9±1.8	89.7±1.5
DGCNN	31.6±2.8	40.8±4.6	19.9±2.1	16.9±1.5
<i>with Single-Modal Pre-Training</i>				
Point-BERT	94.6±3.1	96.3±2.7	91.0±5.4	92.7±5.1
Mask-Point	95.0±3.7	97.2±1.7	91.4±4.0	93.4±3.5
Point-MAE	96.3±2.5	97.8±1.8	92.6±4.1	95.0±3.0
Point-M2AE	96.8±1.8	98.3±1.4	92.3±4.5	95.0±3.0
PointGPT	96.8±2.0	98.6±1.1	92.6±4.6	95.2±3.4
GPM	97.2±2.6	98.7±2.2	92.9±4.2	95.0±3.0
Point-MGE	97.2±1.7	98.7±0.7	92.8±4.0	95.4±3.2
<i>Improvement</i>	+2.6	+2.4	+1.8	+2.7
PointGPT-B	97.5±2.0	98.8±1.0	93.5±4.0	95.8±3.0
Point-MGE-B	97.7±1.8	98.8±0.8	93.8±4.6	95.8±3.4
<i>with Cross-Modal Pre-Training</i>				
ACT	96.8±2.3	98.0±1.4	93.3±4.0	95.6±2.8
Joint-MAE	96.7±2.2	97.9±1.8	92.6±3.7	95.1±2.6
I2P-MAE	97.0±1.8	98.3±1.3	92.6±5.0	95.5±3.0
Recon	97.3±1.9	98.9±1.2	93.3±3.9	95.8±3.0

Table 2: **Few-shot classification on ModelNet40 [Wu et al., 2015].** We report the average accuracy (%) and standard deviation (%) of 10 independent experiments.

probabilities from the generator, we sample and replace those tokens with higher probabilities.

4 Experiments

In this section, we first provide a detailed overview of the pre-training setup of Point-MGE. We then evaluate the pretrained model’s performance in both representation learning and generation capabilities. Finally, to gain a deeper understanding of the roles and importance of each component in the model, we conduct ablation studies on Point-MGE. More results can be found in the Appendix.

4.1 Pre-training Setups

Point-MGE is pre-trained on the ShapeNet [Chang et al., 2015] dataset, which includes 55 different object categories and over 50,000 3D models. From the surface of each 3D shape, 2048 points are uniformly sampled and further divided into 64 patches, each containing 32 points. First, we trained the VQVAE to obtain the discrete tokens. Next, we determined the sliding masking ratio, setting $\beta = 0.5$ and $u = 2$, and pre-trained the ViT-based extractor-generator architecture using multi-scale masked token reconstruction. The number of scales and the number of point patches at each scale were consistent with Point-M2AE [Zhang et al., 2022b]. Additionally, to validate the high-capacity model learning ability of the Point-MGE framework, we scaled the model to ViT-B as described in [Chen et al., 2023], performed post-training, and evaluated its representation learning performance across various downstream tasks. We used

Methods	mIoU _C ↑	mIoU _I ↑
<i>Supervised Learning Only</i>		
PointNet [Qi et al., 2017a]	80.4	83.7
PointNet++ [Qi et al., 2017b]	81.9	85.1
DGCNN [Wang et al., 2019]	82.3	85.2
<i>with Single-Modal Pre-Training</i>		
Transformer + OcCo [Yu et al., 2022]	83.4	85.1
Point-BERT [Yu et al., 2022]	84.1	85.6
Mask-Point [Liu et al., 2022]	84.4	86.0
Point-MAE [Pang et al., 2022]	-	86.1
PointGPT [Chen et al., 2023]	84.1	86.2
GPM [Li et al., 2024]	84.2	85.8
Point-MGE	85.0	86.5
<i>Improvement</i>	+0.9	+0.9
PointGPT-B [Chen et al., 2023]	84.5	86.5
Point-MGE-B	85.0	86.6
<i>with Cross-Modal Pre-Training</i>		
ACT [Dong et al., 2023]	84.7	86.1
Recon [Qi et al., 2023]	84.8	86.4

Table 3: **Part segmentation on ShapeNetPart [Yi et al., 2016].** We report the mean IoU (%) of all part categories (‘mIoU_C’) and the mean IoU of all instances (‘mIoU_I’) in the dataset.

the AdamW optimizer to perform pre-training for 300 epochs. Further implementation details and hyperparameter settings are provided in the Appendix.

4.2 Representation Learning

To demonstrate the representation learning performance of our method, we conducted experiments on shape classification, few-shot learning, and part segmentation. We evaluated the benchmark performance for supervised learning only, single-modal pre-training, and cross-modal pre-training separately.

Shape Classification. We conducted shape classification fine-tuning on two datasets. The ModelNet40 [Wu et al., 2015] dataset includes 3D CAD models of 40 categories, and we followed the official data split provided in [Wu et al., 2015] for our experiments. As shown in Table 1, Point-MGE achieved a second-place classification accuracy of 94.2% on this dataset. The ScanObjectNN [Uy et al., 2019] dataset, derived from real-world indoor scans, contains approximately 15,000 objects across 15 categories. We evaluated this dataset using three different data splits: OBJ-BG, OBJ-ONLY, and PB-T50-RS. The experimental results indicate that Point-MGE consistently outperformed other models across all splits. Notably, in the OBJ-BG setting, Point-MGE achieved an accuracy of 92.9%, outperforming the second-best pre-trained model [Chen et al., 2023] by 1.3 percentage points. Additionally, we extended Point-MGE and three benchmark methods to the ViT-B model for performance evaluation. The results demonstrate that under high-capacity model conditions, our method still maintains a competitive advantage.

Methods	S-FPD ↓	S-KPD ↓ ($\times 10^3$)	R-FID ↓	R-KID ↓ ($\times 10^3$)
Grid-8 ³	4.03	6.15	32.78	14.12
PVD	2.33	2.65	270.64	281.5
3DILG	1.89	2.17	24.83	10.51
3DShape2VecSet	0.97	1.11	24.24	11.76
Point-MGE	0.85	1.34	21.63	11.48

Table 4: **Unconditional generation.** We report four metrics for evaluating the unconditional shape generation task.



Figure 2: **Visualization of unconditional generation.** All models were trained on the complete ShapeNet dataset, and we sampled nine generated results for rendering.

Few-shot Classification. We evaluated the few-shot learning performance of Point-MGE by conducting N-way, K-shot experiments on the ModelNet40 [Wu *et al.*, 2015] dataset. Specifically, we randomly selected N classes from ModelNet40 and sampled K objects from each class. Each experiment was repeated 10 times, and the average and standard deviation of the results were calculated. We evaluated each of the four combinations of settings with $N = \{5, 10\}$ and $K = \{10, 20\}$. As shown in Table 2, under both ViT and ViT-B settings, we achieved SOTA performance in at least three combinations, demonstrating that Point-MGE’s pre-trained 3D representations are highly effective for few-shot learning tasks.

Part Segmentation. Table 3 presents the results of average IoU for all categories ($mIoU_C$) and all instances ($mIoU_I$) in the part segmentation experiments on the ShapeNetPart [Yi *et al.*, 2016] dataset. Compared to the fully supervised method DGCNN [Wang *et al.*, 2019], Point-MGE achieved significant improvements of 2.7% and 1.3% in these two key evaluation metrics, respectively. Our method also outperforms other pre-trained models, achieving a $mIoU_C$ of 85.0%, which ranks first. Additionally, the experimental results show that increasing the number of parameters yields only marginal improvements for this task.

4.3 3D Shape Generation

Unconditional Generation. After completing the pre-training stage, Point-MGE is capable of performing unconditional generation tasks. Fréchet inception distance (FID) and kernel inception distance (KID) are commonly used to evaluate the generation quality of generative models. Following [Zhang *et al.*, 2023a], we use Rendering-FID (R-FID) and Rendering-KID (R-KID) metrics to evaluate the FID and KID of rendered images of 3D shapes, as well as Surface-FPD (S-FPD) and Surface-KPD (S-KPD) metrics to evaluate the FID and KID of sampled point clouds from 3D shapes. Table 4 compares the performance of various methods in uncondi-

	Methods	Airplane	Faucet	Table	Chair
S-FID ↓	3DILG	0.71	2.49	2.10	0.96
	NeuralWavelet	0.38	1.84	1.12	1.14
	3DShape2VecSet	0.62	1.47	1.19	0.76
	Point-MGE	0.67	1.65	1.03	0.71
S-KID ↓ ($\times 10^3$)	3DILG	0.81	3.76	3.84	1.21
	NeuralWavelet	0.53	2.41	1.55	1.50
	3DShape2VecSet	0.83	1.34	1.87	0.70
	Point-MGE	0.79	1.31	1.14	0.58

Table 5: **Category-conditional generation.** We reported the S-FID and S-KID metrics for four categories.



Figure 3: **Visualization of category-conditional generation.** We selected three category labels (airplane, faucet, and table) to display the rendered results of the generated shapes.

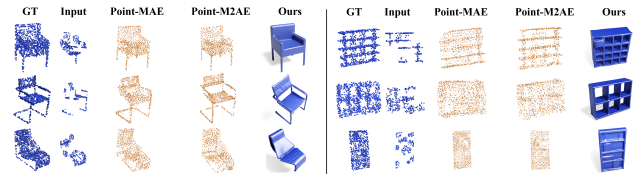


Figure 4: **Visualization of masked point clouds conditional generation.** We used a block masking strategy to mask 70% of the complete point cloud as conditional input. The generated results demonstrated the ability of different models to reconstruct the complete shapes.

Extractor	Generator	Acc (%)	R-FID ↓
6	6	91.2	29.07
8	6	91.9	27.85
12	8	92.4	21.63
12	12	92.1	20.94

Table 6: **Effects of varying transformer depths.** The accuracy (%) on the ScanObjectNN [Uy *et al.*, 2019] (OBJ_BG) and the R-FID for unconditional generation are reported.

tional shape generation on ShapeNet. 3DILG [Zhang *et al.*, 2022a] also adopts a two-stage generation strategy and completes the generation training through an autoregressive process. PVD [Zhou *et al.*, 2021] and 3DShape2VecSet [Zhang *et al.*, 2023a] are generative methods based on diffusion models. Point-MGE outperforms other methods on two of the evaluation metrics, indicating that our approach can generate 3D shapes that closely match the real distribution. Additionally, in Figure 2, we visualize the rendered results of the generated shapes.

Type	Acc (%)	R-FID ↓
Quantized features	92.4	21.63
Index-embedded tokens	87.2	20.34

Table 7: **Effects of input type.** The accuracy (%) and the R-FID are reported.

	Sliding Masking			Various Masking	
	$\beta = 0.5$ $u = 1$	$\beta = 0.5$ $u = 2$	$\beta = 0.7$ $u = 2$	$\mu = 1.0$ $\sigma = 0$	$\mu = 0.7$ $\sigma = 0.25$
Acc (%)	91.9	92.4	91.7	86.2	91.6
R-FID ↓	24.25	21.63	22.71	26.72	22.43

Table 8: **Effects of masking design.** The accuracy (%) and the R-FID are reported.

	NeRFs	EMD	CD L1	CD L2
Acc (%)	92.4	87.9	88.7	89.1
R-FID ↓	21.63	N/A	N/A	N/A

Table 9: **Effects of input type.** The accuracy (%) and the R-FID are reported.

Conditional Generation. We evaluated the conditional generation capabilities of Point-MGE under two different settings. First, we retrained the model using the 54 categories from the ShapeNet [Chang *et al.*, 2015] dataset as conditional embeddings. As shown in Table 5, we evaluated the Surface-FID (S-FID) and Surface-KID (S-KID) for our method and the benchmark methods across four categories. The results indicate that our method achieved performance comparable to or even surpassing those of purely generative approaches. Figure 3 displays the rendered results of generated shapes for three categories (airplane, faucet, and table), with nine instances shown for each category. Next, we further evaluated Point-MGE against other SSL models in the masked generation task. As shown in Figure 4, these models typically train by reconstructing local point clouds, which primarily allows them to complete point cloud reconstruction tasks and depends on the provision of the central point positions. This approach, to some extent, leaks complete shape information to the decoder. In contrast, our method can reconstruct 3D shape meshes using the minimal amount of point cloud information and does not rely on masked center point information during the generation process.

4.4 Ablation Studies

In this section, we discuss several factors that influence the representation learning and generative capabilities of the pre-trained model.

Transformer Depth. As shown in Table 6, we used the standard single scale ViT architecture to build the extractor-generator structure and explored four different transformer depth combinations. The results indicate that increasing the model depth significantly enhances the performance of the pre-trained model. Additionally, consistent with trends ob-

served in previous masked modeling studies [He *et al.*, 2022; Pang *et al.*, 2022; Zhang *et al.*, 2022b], an asymmetric extractor-generator structure is more beneficial for representation learning. This reliance on the extractor to obtain high-quality representations from a small number of visible tokens is due to the use of a relatively simple generator to complete the reconstruction task.

Input Type. In Table 7, we investigate the impact of two different input types on model performance. Specifically, after vector quantizing the initial features of the point cloud patches, we consider using either the quantized features or their indices in the codebook as inputs. Experimental results show that using index-embedded tokens benefits the generation task, but its generalization ability across datasets is limited, which is detrimental to fine-tuning on downstream tasks, leading to poorer representation learning capabilities.

Masking Design. In determining the optimal masking strategy, as shown in Table 8, we compared our sliding masking strategy with the variable masking strategy used in MAGE [Li *et al.*, 2023] and analyzed the impact of different hyperparameters on performance. For the variable masking, μ and σ represent the mean and standard deviation of the truncated Gaussian distribution, respectively. The results indicate that the variable masking ratio, which performs well on 2D images, does not provide an advantage in the point cloud modality, where data is relatively scarce. In contrast, our smooth masking strategy better facilitates the transition between representation learning and generative training.

Reconstruction Target. In exploring the training of VQ-VAE, we compared different reconstruction targets. As shown in Table 9, this study employs NeRFs as the reconstruction target. Additionally, we experimented with directly using point clouds as the reconstruction target and tested methods using Earth Mover’s Distance (EMD) and Chamfer Distance (CD) as loss functions. The experimental results demonstrate that our approach excels in overcoming point cloud sampling bias, leading to superior representation learning capabilities. However, directly using point clouds as the reconstruction target, similar to previous methods, is limited to generating point clouds and cannot produce high-resolution 3D shapes. In the table, this generative capability is marked as Not Applicable (N/A).

5 Conclusion

We present Point-MGE, a novel unified framework for point cloud shape generation and representation learning. Our approach serializes point patches to obtain quantized tokens and applies a sliding masking ratio, allowing it to adapt to both representation learning and generation tasks. Our method excels in addressing the sampling bias issue in point clouds, setting new SOTA results in shape classification, few-shot learning, and part segmentation tasks. Additionally, in generation tasks, our approach achieves near SOTA performance in both unconditional and conditional shape generation, producing realistic high-resolution 3D shapes. We hope our work will draw attention from researchers to the synergistic effects of combining these two model types in 3D vision.

Acknowledgments

This work was supported by the Guangdong Major Project of Basic and Applied Basic Research (2023B0303000016).

References

- [Achlioptas *et al.*, 2018] Panos Achlioptas, Olga Diamanti, Ioannis Mitliagkas, and Leonidas Guibas. Learning representations and generative models for 3d point clouds. In *International conference on machine learning*, pages 40–49. PMLR, 2018.
- [Afham *et al.*, 2022] Mohamed Afham, Isuru Dissanayake, Dinithi Dissanayake, Amaya Dharmasiri, Kanchana Thilakarathna, and Ranga Rodrigo. Crosspoint: Self-supervised cross-modal contrastive learning for 3d point cloud understanding. In *Proceedings of the IEEE/CVF Conference on Computer Vision and Pattern Recognition (CVPR)*, pages 9902–9912, June 2022.
- [Brown *et al.*, 2020] Tom Brown, Benjamin Mann, Nick Ryder, Melanie Subbiah, Jared D Kaplan, Prafulla Dhariwal, Arvind Neelakantan, Pranav Shyam, Girish Sastry, Amanda Askell, et al. Language models are few-shot learners. *Advances in neural information processing systems*, 33:1877–1901, 2020.
- [Chang *et al.*, 2015] Angel X Chang, Thomas Funkhouser, Leonidas Guibas, Pat Hanrahan, Qixing Huang, Zimo Li, Silvio Savarese, Manolis Savva, Shuran Song, Hao Su, et al. Shapenet: An information-rich 3d model repository. *arXiv preprint arXiv:1512.03012*, 2015.
- [Chen and Zhang, 2019] Zhiqin Chen and Hao Zhang. Learning implicit fields for generative shape modeling. In *Proceedings of the IEEE/CVF Conference on Computer Vision and Pattern Recognition (CVPR)*, June 2019.
- [Chen *et al.*, 2023] Guangyan Chen, Meiling Wang, Yi Yang, Kai Yu, Li Yuan, and Yufeng Yue. Pointgpt: Auto-regressively generative pre-training from point clouds. In *Advances in Neural Information Processing Systems*, volume 36, pages 29667–29679, 2023.
- [Cheng *et al.*, 2022] An-Chieh Cheng, Xueting Li, Sifei Liu, Min Sun, and Ming-Hsuan Yang. Autoregressive 3d shape generation via canonical mapping. In *European Conference on Computer Vision*, pages 89–104. Springer, 2022.
- [Chou *et al.*, 2023] Gene Chou, Yuval Bahat, and Felix Heide. Diffusion-sdf: Conditional generative modeling of signed distance functions. In *Proceedings of the IEEE/CVF International Conference on Computer Vision (ICCV)*, pages 2262–2272, October 2023.
- [Devlin *et al.*, 2018] Jacob Devlin, Ming-Wei Chang, Kenton Lee, and Kristina Toutanova. Bert: Pre-training of deep bidirectional transformers for language understanding. *arXiv preprint arXiv:1810.04805*, 2018.
- [Dhariwal and Nichol, 2021] Prafulla Dhariwal and Alexander Nichol. Diffusion models beat gans on image synthesis. *Advances in neural information processing systems*, 34:8780–8794, 2021.
- [Dinh *et al.*, 2014] Laurent Dinh, David Krueger, and Yoshua Bengio. Nice: Non-linear independent components estimation. *arXiv preprint arXiv:1410.8516*, 2014.
- [Dong *et al.*, 2023] Runpei Dong, Zekun Qi, Linfeng Zhang, Junbo Zhang, Jianjian Sun, Zheng Ge, Li Yi, and Kaisheng Ma. Autoencoders as cross-modal teachers: Can pre-trained 2d image transformers help 3d representation learning? In *The Eleventh International Conference on Learning Representations*, 2023.
- [Guo *et al.*, 2023] Ziyu Guo, Renrui Zhang, Longtian Qiu, Xianzhi Li, and Pheng-Ann Heng. Joint-mae: 2d-3d joint masked autoencoders for 3d point cloud pre-training. In *Proceedings of the Thirty-Second International Joint Conference on Artificial Intelligence*, pages 791–799, 2023.
- [He *et al.*, 2022] Kaiming He, Xinlei Chen, Saining Xie, Yanghao Li, Piotr Dollár, and Ross Girshick. Masked autoencoders are scalable vision learners. In *Proceedings of the IEEE/CVF conference on computer vision and pattern recognition*, pages 16000–16009, 2022.
- [Hui *et al.*, 2022] Ka-Hei Hui, Ruihui Li, Jingyu Hu, and Chi-Wing Fu. Neural wavelet-domain diffusion for 3d shape generation. In *SIGGRAPH Asia 2022 Conference Papers*, pages 1–9, 2022.
- [Ibing *et al.*, 2021] Moritz Ibing, Isaak Lim, and Leif Kobbelt. 3d shape generation with grid-based implicit functions. In *Proceedings of the IEEE/CVF Conference on Computer Vision and Pattern Recognition (CVPR)*, pages 13559–13568, June 2021.
- [Li *et al.*, 2023] Tianhong Li, Huiwen Chang, Shlok Mishra, Han Zhang, Dina Katabi, and Dilip Krishnan. Mage: Masked generative encoder to unify representation learning and image synthesis. In *Proceedings of the IEEE/CVF Conference on Computer Vision and Pattern Recognition (CVPR)*, pages 2142–2152, June 2023.
- [Li *et al.*, 2024] Zhe Li, Zhangyang Gao, Cheng Tan, Bocheng Ren, Laurence T Yang, and Stan Z Li. General point model pretraining with autoencoding and autoregressive. In *Proceedings of the IEEE/CVF Conference on Computer Vision and Pattern Recognition*, pages 20954–20964, 2024.
- [Liu *et al.*, 2022] Haotian Liu, Mu Cai, and Yong Jae Lee. Masked discrimination for self-supervised learning on point clouds. In *European Conference on Computer Vision*, pages 657–675. Springer, 2022.
- [Ma *et al.*, 2022] Xu Ma, Can Qin, Haoxuan You, Haoxi Ran, and Yun Fu. Rethinking network design and local geometry in point cloud: A simple residual MLP framework. In *International Conference on Learning Representations*, 2022.
- [Mittal *et al.*, 2022] Paritosh Mittal, Yen-Chi Cheng, Ma-neesh Singh, and Shubham Tulsiani. Autosdf: Shape priors for 3d completion, reconstruction and generation. In *Proceedings of the IEEE/CVF Conference on Computer Vision and Pattern Recognition (CVPR)*, pages 306–315, June 2022.

- [Morton, 1966] Guy M Morton. A computer oriented geodesic data base and a new technique in file sequencing. 1966.
- [Pang *et al.*, 2022] Yatian Pang, Wenxiao Wang, Francis EH Tay, Wei Liu, Yonghong Tian, and Li Yuan. Masked autoencoders for point cloud self-supervised learning. In *European conference on computer vision*, pages 604–621. Springer, 2022.
- [Qi *et al.*, 2017a] Charles R. Qi, Hao Su, Kaichun Mo, and Leonidas J. Guibas. Pointnet: Deep learning on point sets for 3d classification and segmentation. In *Proceedings of the IEEE Conference on Computer Vision and Pattern Recognition (CVPR)*, July 2017.
- [Qi *et al.*, 2017b] Charles Ruizhongtai Qi, Li Yi, Hao Su, and Leonidas J Guibas. Pointnet++: Deep hierarchical feature learning on point sets in a metric space. *Advances in neural information processing systems*, 30, 2017.
- [Qi *et al.*, 2023] Zekun Qi, Runpei Dong, Guofan Fan, Zheng Ge, Xiangyu Zhang, Kaisheng Ma, and Li Yi. Contrast with reconstruct: Contrastive 3d representation learning guided by generative pretraining. In *International Conference on Machine Learning*, pages 28223–28243. PMLR, 2023.
- [Rezende and Mohamed, 2015] Danilo Rezende and Shakir Mohamed. Variational inference with normalizing flows. In *International conference on machine learning*, pages 1530–1538. PMLR, 2015.
- [Shue *et al.*, 2023] J. Ryan Shue, Eric Ryan Chan, Ryan Po, Zachary Ankner, Jiajun Wu, and Gordon Wetzstein. 3d neural field generation using triplane diffusion. In *Proceedings of the IEEE/CVF Conference on Computer Vision and Pattern Recognition (CVPR)*, pages 20875–20886, June 2023.
- [Touvron *et al.*, 2023] Hugo Touvron, Louis Martin, Kevin Stone, Peter Albert, Amjad Almahairi, Yasmine Babaei, Nikolay Bashlykov, Soumya Batra, Prajjwal Bhargava, Shrutu Bhosale, et al. Llama 2: Open foundation and fine-tuned chat models. *arXiv preprint arXiv:2307.09288*, 2023.
- [Uy *et al.*, 2019] Mikaela Angelina Uy, Quang-Hieu Pham, Binh-Son Hua, Thanh Nguyen, and Sai-Kit Yeung. Revisiting point cloud classification: A new benchmark dataset and classification model on real-world data. In *Proceedings of the IEEE/CVF International Conference on Computer Vision (ICCV)*, October 2019.
- [Vahdat *et al.*, 2022] Arash Vahdat, Francis Williams, Zan Gojcic, Or Litany, Sanja Fidler, Karsten Kreis, et al. Lion: Latent point diffusion models for 3d shape generation. *Advances in Neural Information Processing Systems*, 35:10021–10039, 2022.
- [Van Den Oord *et al.*, 2017] Aaron Van Den Oord, Oriol Vinyals, et al. Neural discrete representation learning. *Advances in neural information processing systems*, 30, 2017.
- [Vaswani *et al.*, 2017] Ashish Vaswani, Noam Shazeer, Niki Parmar, Jakob Uszkoreit, Llion Jones, Aidan N Gomez, Łukasz Kaiser, and Illia Polosukhin. Attention is all you need. *Advances in neural information processing systems*, 30, 2017.
- [Wang *et al.*, 2019] Yue Wang, Yongbin Sun, Ziwei Liu, Sanjay E Sarma, Michael M Bronstein, and Justin M Solomon. Dynamic graph cnn for learning on point clouds. *ACM Transactions on Graphics (tog)*, 38(5):1–12, 2019.
- [Wang *et al.*, 2022] Ziyi Wang, Xumin Yu, Yongming Rao, Jie Zhou, and Jiwen Lu. P2p: Tuning pre-trained image models for point cloud analysis with point-to-pixel prompting. *Advances in neural information processing systems*, 35:14388–14402, 2022.
- [Wei *et al.*, 2022] Chen Wei, Haoqi Fan, Saining Xie, Chao-Yuan Wu, Alan Yuille, and Christoph Feichtenhofer. Masked feature prediction for self-supervised visual pre-training. In *Proceedings of the IEEE/CVF Conference on Computer Vision and Pattern Recognition (CVPR)*, pages 14668–14678, June 2022.
- [Wu *et al.*, 2015] Zhirong Wu, Shuran Song, Aditya Khosla, Fisher Yu, Linguang Zhang, Xiaoou Tang, and Jianxiong Xiao. 3d shapenets: A deep representation for volumetric shapes. In *Proceedings of the IEEE Conference on Computer Vision and Pattern Recognition (CVPR)*, June 2015.
- [Xie *et al.*, 2016] Jianwen Xie, Yang Lu, Song-Chun Zhu, and Yingnian Wu. A theory of generative convnet. In *International Conference on Machine Learning*, pages 2635–2644. PMLR, 2016.
- [Xie *et al.*, 2020a] Jianwen Xie, Zilong Zheng, Ruiqi Gao, Wenguan Wang, Song-Chun Zhu, and Ying Nian Wu. Generative voxelnet: Learning energy-based models for 3d shape synthesis and analysis. *IEEE Transactions on Pattern Analysis and Machine Intelligence*, 44(5):2468–2484, 2020.
- [Xie *et al.*, 2020b] Saining Xie, Jiatao Gu, Demi Guo, Charles R Qi, Leonidas Guibas, and Or Litany. Point-contrast: Unsupervised pre-training for 3d point cloud understanding. In *Computer Vision—ECCV 2020: 16th European Conference, Glasgow, UK, August 23–28, 2020, Proceedings, Part III 16*, pages 574–591. Springer, 2020.
- [Xie *et al.*, 2021] Jianwen Xie, Yifei Xu, Zilong Zheng, Song-Chun Zhu, and Ying Nian Wu. Generative pointnet: Deep energy-based learning on unordered point sets for 3d generation, reconstruction and classification. In *Proceedings of the IEEE/CVF Conference on Computer Vision and Pattern Recognition (CVPR)*, pages 14976–14985, June 2021.
- [Yan *et al.*, 2022] Xingguang Yan, Liqiang Lin, Niloy J. Mitra, Dani Lischinski, Daniel Cohen-Or, and Hui Huang. Shapeformer: Transformer-based shape completion via sparse representation. In *Proceedings of the IEEE/CVF Conference on Computer Vision and Pattern Recognition (CVPR)*, pages 6239–6249, June 2022.
- [Yang *et al.*, 2019] Guandao Yang, Xun Huang, Zekun Hao, Ming-Yu Liu, Serge Belongie, and Bharath Hariharan.

- Pointflow: 3d point cloud generation with continuous normalizing flows. In *Proceedings of the IEEE/CVF international conference on computer vision*, pages 4541–4550, 2019.
- [Yi *et al.*, 2016] Li Yi, Vladimir G Kim, Duygu Ceylan, I-Chao Shen, Mengyan Yan, Hao Su, Cewu Lu, Qixing Huang, Alla Sheffer, and Leonidas Guibas. A scalable active framework for region annotation in 3d shape collections. *ACM Transactions on Graphics (ToG)*, 35(6):1–12, 2016.
- [Yu *et al.*, 2022] Xumin Yu, Lulu Tang, Yongming Rao, Tiejun Huang, Jie Zhou, and Jiwen Lu. Point-bert: Pre-training 3d point cloud transformers with masked point modeling. In *Proceedings of the IEEE/CVF Conference on Computer Vision and Pattern Recognition (CVPR)*, pages 19313–19322, June 2022.
- [Zhang *et al.*, 2021] Zaiwei Zhang, Rohit Girdhar, Armand Joulin, and Ishan Misra. Self-supervised pretraining of 3d features on any point-cloud. In *Proceedings of the IEEE/CVF International Conference on Computer Vision (ICCV)*, pages 10252–10263, October 2021.
- [Zhang *et al.*, 2022a] Biao Zhang, Matthias Nießner, and Peter Wonka. 3dilg: Irregular latent grids for 3d generative modeling. volume 35, pages 21871–21885, 2022.
- [Zhang *et al.*, 2022b] Renrui Zhang, Ziyu Guo, Peng Gao, Rongyao Fang, Bin Zhao, Dong Wang, Yu Qiao, and Hongsheng Li. Point-m2ae: multi-scale masked autoencoders for hierarchical point cloud pre-training. *Advances in neural information processing systems*, 35:27061–27074, 2022.
- [Zhang *et al.*, 2023a] Biao Zhang, Jiapeng Tang, Matthias Niessner, and Peter Wonka. 3dshape2vecset: A 3d shape representation for neural fields and generative diffusion models. *ACM Transactions on Graphics (TOG)*, 42(4):1–16, 2023.
- [Zhang *et al.*, 2023b] Renrui Zhang, Liuhui Wang, Yu Qiao, Peng Gao, and Hongsheng Li. Learning 3d representations from 2d pre-trained models via image-to-point masked autoencoders. In *Proceedings of the IEEE/CVF Conference on Computer Vision and Pattern Recognition*, pages 21769–21780, 2023.
- [Zheng *et al.*, 2022] Xinyang Zheng, Yang Liu, Pengshuai Wang, and Xin Tong. Sdf-stylegan: Implicit sdf-based stylegan for 3d shape generation. In *Computer Graphics Forum*, volume 41, pages 52–63. Wiley Online Library, 2022.
- [Zhou *et al.*, 2021] Linqi Zhou, Yilun Du, and Jiajun Wu. 3d shape generation and completion through point-voxel diffusion. In *Proceedings of the IEEE/CVF international conference on computer vision*, pages 5826–5835, 2021.